



Dynamic interplay between metal nanoparticles and oxide support under redox conditions

Journal Article

Author(s):

Frey, Hannes ; Beck, Arik; Huang, Xing ; van Bokhoven, Jeroen Anton; Willinger, Marc-Georg

Publication date:

2022

Permanent link:

<https://doi.org/10.3929/ethz-b-000549975>

Rights / license:

[Creative Commons Attribution 4.0 International](#)

Originally published in:

Science 376(6596), <https://doi.org/10.1126/science.abm3371>

Funding acknowledgement:

181053 - Elektronenmikroskopische Untersuchungen zur Dynamik von Metall- Träger Wechselwirkungen unter katalytisch Relevanten Bedingungen (SNF)

178943 - Catalyst structures in three dimensions (SNF)

Dynamic interplay between metal nanoparticles and oxide support under redox conditions

Authors: Frey, H.^{1,2†}, Beck, A.^{2,3†}, Huang, X.^{1,4*}, van Bokhoven, J. A.^{2,3*}, Willinger, M. G.^{1*}

Affiliations:

5 ¹Scientific Center of Optical and Electron Microscopy (ScopeM) ETH Zürich; 8093 Zürich, Switzerland

²Institute for Chemical and Bioengineering, ETH Zürich; 8093 Zürich, Switzerland

10 ³Paul Scherrer Institute; 5232 Villigen, Switzerland

⁴College of Chemistry, Fuzhou University, Fuzhou 350116, P. R. China.

[†]The authors contributed equally to the work.

15

*Corresponding Authors. Email addresses: xinghuang@fzu.edu.cn,
jeroen.vanbokhoven@chem.ethz.ch, marc.willinger@tum.de

20

Abstract:

The dynamic interactions between noble metal particles and reducible metal-oxide supports can depend on redox reactions with ambient gases. Transmission electron microscopy revealed that the strong metal support interaction (SMSI) induced encapsulation of platinum particles on titania

observed under reducing conditions is lost once the system is exposed to a redox-reactive environment of oxygen and hydrogen mixture at a pressure of around 1bar. Direct observation showed that destabilization of the metal-oxide interface and redox mediated reconstructions of titania leads to particle dynamics and directed particle migration that depend on nanoparticle orientation. The encapsulated and static SMSI state was re-established when switching back to purely oxidizing conditions. This work thus highlights the difference between reactive and nonreactive state and demonstrates that the manifestation of the metal-support interaction and state of a catalyst strongly depends on the chemical environment.

One-Sentence Summary: Real-time atomic scale observations reveal the state of an SMSI system under reactive conditions and show that redox induced processes at the metal-support interface determine the dynamic behavior of the catalyst.

Noble metal nanoparticles (NPs) are used as active constituents of catalysts and thus play an important role in the sustainable production of chemicals and fuels, and the mitigation of pollutants. The interesting catalytic properties of noble metals emerge when dispersed as nanometer-sized particles on high-surface area oxide supports. Although simple models attribute catalytic properties mainly to size effects, with the metal being the active phase on an inert oxide support, it is known that synergistic interactions between metal and support can be critical (1, 2).

A dramatic example of metal-support interactions is the loss of hydrogen chemisorption of titania-supported platinum (Pt/TiO₂) upon high-temperature reductive treatment (HTR). The effect, first observed by Tauster *et al.* (3), can be reverted through a series of high temperature oxidation and subsequent low temperature reduction steps (3). Originally, the chemisorption suppression was attributed to an electronic perturbation of the system, that is, the bonding between Pt and Ti cations under reducing atmospheres. Subsequent studies showed that in situ reductive activation leads to encapsulation of Pt NPs particles in a thin, partially reduced layer of TiO₂ (4–10). The driving force for this so-called strong metal-support interaction (SMSI) state was attributed to surface energy minimization (11).

Similar encapsulation effects have also been reported for cobalt (12), nickel (13, 14), gold (15) and copper (16) NPs. More recently, it was shown that high-temperature oxidative treatment can also lead to NP encapsulation (15, 17–20). Potential benefits of SMSI encapsulation include enhanced resistivity against both NP coalescence and Ostwald ripening (21–23). Furthermore, the selectivity of the catalyst can be tuned by modifying the adsorption strength of molecules on the catalyst surface and by blocking specific active sites (24–28). Hence, the ability to exploit synergistic interactions between metal NPs and their support in a controlled way is of high interest with regards to the development of improved catalysts and processes.

Early studies on the SMSI were mostly based on indirect, integral spectroscopic observations and provided evidence of NP encapsulation either through an altered chemical composition of the surface or through SMSI-induced changes in the chemisorption capacity. High-resolution real-space methods, such as scanning tunneling microscopy (STM) and transmission electron microscopy (TEM), can provide direct atomic-scale imaging to confirm the formation of the encapsulating SMSI state after high-temperature reductive (29–31) or, respectively, oxidizing treatment (4). However, because of methodological constraints, direct imaging of the encapsulated state has mostly been achieved ex situ, in experiments where the SMSI state was preserved during cooling and sample transfer from catalytic reactor to the high-vacuum environment of a microscope. Despite detailed characterization of preserved SMSI states, little is known about metal-support interactions under catalytic reaction conditions.

Because the chemical state of metal particle and reducible support are influenced by the chemical environment (32, 33), their mutual interaction and possible synergistic effects should be investigated under working conditions. Direct real-space observations by in situ STM and environmental TEM have shown gas-phase induced reconstruction of NPs (34–37) and changes at the metal-support interface (38). Environmental TEM is generally limited to chamber pressures of around 20 mbar (39). Depending on the system studied, the pressure-dependent chemical potential of reactive species might thus be too low to trigger specific processes and reactions that are relevant for catalytic function at higher pressure. However, the development and commercial availability of microelectromechanical (MEMS)-based reactors for in situ electron microscopy has extended the accessible pressure range by roughly two orders of magnitude (11, 40, 41) and enabled to partially bridge the so-called pressure gap (42).

This study builds on earlier investigations of interfacial dynamics on oxide-supported noble metal NPs (38, 43, 44). Working at higher pressure allows us to visualize gas-phase induced

processes that are directly linked to metal-support interactions and revealed the dynamic interplay between NP support and gas phase under working conditions. We selected a Pt/TiO₂ catalyst because it is the archetype system for which the SMSI state was first described (3), and for which we have recently shown that a static encapsulated state of Pt NPs not only exists under hydrogen, but also under purely oxidizing conditions, however, with a specific overlayer structure that depends on the gas environment (4). We studied hydrogen oxidation because it is the most elementary redox reaction that can also be viewed as a representation of many reactions, such as partial hydrocarbon oxidations. Furthermore, this catalytic system only yields water in gas phase reactions at high temperatures (45). Our in situ TEM-based study revealed how the classical encapsulated SMSI state of Pt can be lost through destabilization of the overlayer once the system is exposed to a redox-active regime in which H₂ and O₂ are simultaneously interacting with the catalyst.

Under reaction conditions, we observed interfacial dynamics that are characterized by local structural collapse and rebuilding of TiO₂, i.e., redox processes involving the reduction and subsequent re-oxidation of the support underneath Pt NPs. In this process, the inherent lattice mismatch between Pt and TiO₂ and the associated interfacial strain lowers the barrier for vacancy formation in the reducible oxide. The resulting interfacial reconstructions give rise to pronounced changes in particle morphology and, eventually, particle mobility. Previous studies in which purely reducing or oxidizing ambients were used, did not show such dynamics and were not representative of reaction conditions (4, 11, 46, 47). Water, which is formed as reaction product is not the cause of the observed phenomena. Instead, addition of water to the feed suppresses particle dynamics. Relevant for the NP behavior is the configuration of the metal-support interface, as shown for three selected cases of differently oriented NPs. This work provides an explanation for the observed particle restructuring and directed particle migration on the support. Furthermore, it provides

additional evidence for a nonclassical SMSI-state that is observed in oxidizing conditions (17, 20, 48).

Results

5 *1. Switching to a redox-active H₂-O₂ mixture*

We investigated the metal-support interactions and the relevance of an SMSI encapsulated state under redox conditions. TiO₂-supported Pt NPs were first heated in H₂ in order to induce the classical SMSI state and then transferred under inert gas purging into an O₂ atmosphere. As described in (4) and detailed in the experimental part (see supporting information), this treatment led to Pt NPs in a non-classical oxidized SMSI state. Once prepared, the system was transited into the relevant redox reactive regime through addition of H₂ into the O₂ flow. This sequence led to a gradual change in the encapsulated state of the Pt NPs and finally, complete removal of the overlayer (Fig. 1, A to F). The first observable effect that could be attributed to an increasing partial pressure of H₂ in the reactor was the onset of overlayer reduction. It was detected as an instant change in the overlayer structure on the (001) facet (see **movie S1**), followed by retraction of the overlayer on the (111) plane (**Fig. 1**). The latter initiated near an uncovered Pt{110}-type microfacet, as indicated by the propagating reduction front in the image sequence of **Fig. 1, G to I** (see also **movie S2**). Within seconds, the overlayer vanished from the Pt{111} surfaces, whereas some transient patches, selectively decorating Pt{100} planes, could still be observed (see **Fig. 1, C and D**, and **movies S1 and S2**). Similar transiently existing nanopatches were observed for the Pt/TiO₂ system in field ion microscopy (49) and were reported for iron oxide-supported Pt NPs (50).

Once the gas composition reached a set mixture (60 mbar H₂ and 700 mbar O₂) after about 180 s, the encapsulating overgrowth layer was fully retracted from all particles. Thus, stable

configurations of static Pt particles exhibiting encapsulating layers existed either in pure H₂ (the classical SMSI state) or in pure O₂ (the non-classical SMSI state), but not in a regime where both gases were simultaneously present. Signs of the structural incompatibility between the reduced and oxidized overlayer on the Pt particles could also be detected at the remaining NP-support interface (see below). With the removal of the overlayer, Pt NPs furthermore underwent a shape change through a slight expansion of {100} facets (see **Fig. 1 A, G, and F** and structure model in **Fig. S3**). Once the overlayer was fully removed, the onset of pronounced particle dynamics involving restructuring and migration was observed (see image sequence in **Fig. 1, E and F, and movie S1**).

2. Particle and interfacial dynamics in the redox-active regime

Movies recorded at lower magnification showed the response of a collection of NPs to reaction conditions. As shown in **movie S3**, the degree of structural dynamics and mobility differed between NPs. Some NPs remained static, whereas others underwent structural fluctuations; some remained stationary, whereas others migrated across the substrate surface. These individual dynamics indicate that each NP responded according to local surface topological features and the configuration of the interface.

Because rutile TiO₂ preferentially exposes low-energy {110} facets (51), and Pt NPs were generally present in the form of truncated cuboctahedra, exposing mostly {100} and {111} facets, only a limited number of interface configurations need to be considered for a general description of the observed behavior. Indeed, a preferential orientation relationship between the Pt NP and the support is evident from the analysis of lattice fringes of isolated Pt NPs that are attached to the same TiO₂ particle. As shown in **Fig. 2E** and the corresponding colorized lattice fringes in the Fourier-filtered image in **Fig. 2 F** and **Fig. S4**, the particles show identical orientation of their

(111) and (100) planes and thus, preferential orientation driven by a minimization of the lattice misfit induced interfacial strain.

The first NP we considered (**Fig. 2, A to C**) was oriented with Pt{111} planes perpendicular to the Pt/TiO₂ interface. Images recorded after overlayer retraction showed occasional slight rotations of the NP. Such slight rotations could be induced by reconstructions at the interface, similar to the recently reported case of gas-phase induced rotation of gold NPs on a TiO₂ support, which was observed by low-pressure environmental TEM (43). With increasing H₂ partial pressure, the Pt NP developed pronounced structural dynamics that involved twin-formation and shearing along Pt{111} planes in an up-down motion, perpendicular to the Pt/TiO₂ interface (see arrows in **Fig. 2C**). This up-down motion can be seen in **Fig. 2D**, which was generated by cutting a plane through the recorded image stack along the time axis, and is also shown in **movie S4**.

These structural dynamics at the interface imply that the TiO₂ substrate locally collapsed, and at a later point in time, was rebuilt. The cross-section view provided by TEM imaging showed a substantial reshuffling of material at the interface, with Pt 111 planes moving up and down in response. Characteristic for this process is the pronounced formation of {111}-twinning planes, which has also been observed for the case of zinc oxide-supported copper NPs in a redox environment (52).

The second case, shown in **Fig. 2 G to J** and **movie S5**, represents NPs in which Pt{111} planes were oriented almost parallel to the Pt/TiO₂ interface. Here, a repetitive forward- and backward- step-flow-like motion of Pt{111} planes was observed. Similar to the case of Pt{111}-planes moving up- and downwards in **Fig. 2, A to C**, this motion could be caused by similar redox processes, rotated by 90 ° and without the involvement of twinning-planes running through the Pt NP.

The third case we considered was a Pt NP oriented with a {001}-plane parallel to the Pt/TiO₂ interface. Because TEM images only show a 2D projection of a 3D object, the precise location of the interface was not clear in **Fig. 2, K to N**. Nevertheless, we could follow the shape evolution of the moving NP with time and abstract information about the ongoing processes. The NP exposed Pt{111} planes that were inclined with respect to the interface. At times, microfaceting of the (111) plane was observed at the right side of the particle, which, in effect, tilted it down toward the substrate (see **Fig. 2 K**). Moments later, the right side reconstructed until a planar {111} facet was restored. This downward-inclination and subsequent retraction occurred repetitively, whereas the opposing (111) plane on the left side, which faced away from the substrate, did not show any change. The reshuffling of Pt at one end was responsible for a net transport of Pt from the right (back side) to the left (front side) and resulted in a propagating motion. This redox chemistry-driven directional migration of the Pt NP is shown in **movie S6**.

These three cases show how the relative orientation of Pt NP and the TiO₂ support can be linked to the behavior of individual NP. Depending on the configuration of the interface, the underlying redox processes can give rise either to Pt NPs that restructure and do not move, or to NP that restructure and migrate on the surface in a directed manner.

3. Retraction of H₂ and re-formation of the oxidic SMSI overlayer

When we switched the gas composition back from a reactive to a purely oxidizing regime by turning off the H₂ flow, an encapsulated state of Pt NPs was re-established. The first apparent effect of a reduced H₂ concentration was a sudden morphological change of the Pt NPs toward a more spherical shape, typical for the effect of O₂ (33) (see **Fig. 3, A to C**, and **movie S7**). Subsequently, the migration of support material onto the Pt NPs and thus, reformation of the overgrowth layer was observed. The image sequence in **Fig. 3, D to F**, showed that NP coverage started at the Pt/TiO₂ interface and propagated upward. The support underneath showed a weakening of image

contrast in the vicinity of the Pt NP (see **Fig. 3 D**), indicating that the material forming the overlayer originated from there. Electron energy loss spectroscopy (EELS) measurements confirmed that the overlayer consisted of TiO₂ (**Fig. S5**).

Once the coverage was restored, all of the dynamical effects ceased and the system reached a static state. Because water was formed as reaction product and could influence the above described particle dynamics, further experiments were performed in which water vapor was co-fed first to an O₂-containing atmosphere (up to p_{H₂O} ~ 20 mbar, see SI) and subsequently, to a mixture of O₂ (700 mbar) and H₂ (120 mbar) at 600°C. **Movie S8** showed that neither particle dynamics nor migration was observed as a consequence of the added water vapor. Only after retracting water from the feed gas did particle dynamics reemerge (**Movie S8** and **Fig. S6**).

Discussion

This work was motivated by questions regarding the relevance of the classical SMSI state beyond reductive activation and thus, the behavior of the system under reactive conditions. Encapsulation is often used to explain the altered behavior of supported metal NPs, although it represents a state obtained after HTR or, as recently shown, treatment in O₂. Little is known about the SMSI state under reaction conditions and its relation to catalytic function.

Starting with encapsulated NPs in an oxidizing atmosphere, the key finding of this work is that exposure to a redox active environment led to the removal of the overlayer and subsequently, the emergence of particle dynamics. Thus, the classical SMSI state was lost as soon as the surface was exposed to a reactive atmosphere. The absence of an overlayer indicated that neither the reduced TiO₂ overlayer found in H₂, nor the oxidized version found in O₂, was stable under redox conditions. The simultaneous presence of reducing and oxidizing agents induced redox processes

that lead to destabilization and overlayer retraction. Hydrogen is easily activated on platinum, but activation on TiO₂ is much more unlikely (53–55). Its addition to the feed gas triggered oxygen abstraction from the overlayer, thereby destabilizing and finally stripping it from the particle surface.

5 The areal increase of Pt{100} facets upon overlayer retraction suggested that H₂, despite a presumably low equilibrium coverage at 600°C and 60 mbar (56), dominated the NP shape. Indirect evidence for activation of H₂ on Pt is provided by **Fig. 1, G to I**, and in the **movie S2**, where overlayer retraction was initiated at a kink in the NP and propagated from there across the Pt surface. A similar mechanism was observed for the reduction of an O-Fe-O trilayer on an
10 extended Pt{111} surface during CO oxidation (57).

Redox-induced processes not only destabilized the encapsulating layer, but also acted at the remaining Pt/TiO₂ interface and led to pronounced particle dynamics. Structural incoherence of Pt and TiO₂ (58) created inhomogeneous strain at the NP-support interface (59). The strain was modulated with a periodicity of the moiré or coincidence lattice (60). Strain modulation locally
15 reduced the energetic costs for oxygen vacancy formation in the reducible support (60, 61). Experimentally, similar strain-facilitated introduction of oxygen vacancies at the NP-support interface under reducing conditions was observed for a cerium oxide–rhodium model catalyst (60), and a gold ceria interface, (62) and furthermore predicted by DFT for Pt on TiO₂ (63).

20 In rutile, aggregation of oxygen vacancies is energetically favored and leads to shear plane formation. These so-called Wadsley defects (64–68) can form already at low oxygen deficiencies (69). The introduction of shear planes reduces the elastic energy density stored in the interface (59) and prompts a morphology adaptation of the supported particle. With increasing extent of reduction, the local affinity of TiO_x toward re-oxidation increases (70) up to the point where re-oxidation takes place and induces, once again, morphological adaption of the Pt NPs. This redox-

mediated reconstruction can be seen in **Movie S4**, which shows the periodic collapse and rebuilding of the TiO₂ structure underneath a Pt NP. In a simplified model, the process can be viewed as an oscillator in which energy is transferred back and forth between strain/misfit- and chemical energy. The process is driven by competing actions of H₂ and O₂ and enabled by a sufficiently high temperature and chemical potential of the constituent gasses. Such atmosphere-induced reconstructions have been revealed by HRTEM in dilute atmospheres, and were reported for the case of gold on gamma-iron oxide, gold on TiO₂, gold on ceria, and platinum on iron oxide (37, 43, 71, 72). In all of these cases, a change in interface configuration, expressed as either a rotational movement of the particle relative to the interface (43), or a stepwise translational motion (37) was detected.

Our work bridges the pressure-gap from the low-pressure, quasi-static regime to a regime where the chemical potential of the involved species (H₂ and O₂) is sufficient to induce more substantial redox dynamics. At the applied pressure, activated hydrogen can easily remove oxygen from the underlying TiO₂ support (53). Overall, this process resembles the Mars van Krevelen mechanism, as oxygen from the catalyst ends up in the product (73). However, it is not restricted to surface reduction and oxidation. Our in situ observations show that, depending on the relative orientation of particle and support, interfacial reconstructions result in different particle dynamics. The three representative cases presented here show that interface-reconstructions promoted formation of twin-boundaries and step-flow growth and retraction at Pt{111} gliding planes, and can give rise to directional surface migration of Pt NPs. Under redox conditions, particle dynamics and surface migration are thus largely driven by chemical processes and determined by orientation relationships, surface structure, and topology. In this way, the migration behavior of particles can be rationalized.

The observed oscillatory behavior reflected the bistability associated to redox processes and inability of the system to settle as long as a reactive state was maintained. Water, when present in excess, did not induce any dynamics, but rather quenched them. Water preferably dissociates at oxygen vacancies (74) and, when added in excess, worked against TiO₂ reduction by shifting the redox regime to higher temperatures. When the feed is switched back to dry H₂ plus O₂, particle dynamics re-emerged until finally, the dynamics were stopped when H₂ was removed from the feed. At that moment, a static overlayer reformed. The system thus equilibrated by reverting to an oxygen-induced SMSI state, that was formed in this case directly, without prior initialization through the well-known high-temperature reduction route. This nonclassical, oxygen-induced SMSI state was recently observed by Tang *et. al.* (20).

The dynamic behavior described in this work remained unnoticed in ex situ and post-mortem studies, highlighting the importance of in situ observations. The complex interplay between metal and support under reaction conditions that was described here for the model reaction of H₂ oxidation shows how synergistic interactions emerge at strained interfaces between metal and reducible support and provide a means for lowering oxidation barriers. Since these effects are influenced by the local structure of the interface of each individual particle, those insights are even hidden for integral in situ methods that average over a large fraction of a sample. The reported individual behavior and its correlation to structure has to be included into models that aim to describe overall structural transformations of a catalyst under redox conditions. Theory may then provide insight into how the dynamic behavior and interfacial redox processes lead to formation and disappearance of active sites that link the restructuring and motion directly to the reaction kinetics.

References and Notes

1. M. Haruta, Size- and support-dependency in the catalysis of gold. *Catal. Today*. **36**, 153–166 (1997).
2. T. W. van Deelen, C. Hernández Mejía, K. P. de Jong, Control of metal-support interactions in heterogeneous catalysts to enhance activity and selectivity. *Nat. Catal.* **2**, 955–970 (2019).
3. S. J. Tauster, S. C. Fung, R. L. Garten, Strong metal-support interactions. Group 8 noble metals supported on titanium dioxide. *J. Am. Chem. Soc.* **100**, 170–175 (1978).
4. A. Beck, X. Huang, L. Artiglia, M. Zabilskiy, X. Wang, P. Rzepka, D. Palagin, M.-G. Willinger, J. A. van Bokhoven, The dynamics of overlayer formation on catalyst nanoparticles and strong metal-support interaction. *Nat. Commun.* **11**, 3220 (2020).
5. W. Zhao, D. Zhou, S. Han, Y. Li, J. Liu, Y. Zhou, M. Li, X. Zhang, W. Shen, Metal–Support Interaction in Pt/TiO₂: Formation of Surface Pt–Ti Alloy. *J. Phys. Chem. C*. **125**, 10386–10396 (2021).
6. X. Wang, A. Beck, J. A. van Bokhoven, D. Palagin, Thermodynamic insights into strong metal–support interaction of transition metal nanoparticles on titania: simple descriptors for complex chemistry. *J. Mater. Chem. A*. **9**, 4044–4054 (2021).
7. D. N. Belton, Y. M. Sun, J. M. White, Thin-film models of strong metal-support interaction catalysts. Platinum on oxidized titanium. *J. Phys. Chem.* **88**, 1690–1695 (1984).
8. C. S. Ko, R. J. Gorte, Evidence for Diffusion of a Partially Oxidized into Bulk Platinum. *J. Catal.* **90**, 59–64 (1984).
9. R. A. Demmin, C. S. Ko, R. J. Gorte, Effect of titania on the chemisorption and reaction properties of platinum. *J. Phys. Chem.* **89**, 1151–1154 (1985).

10. S. Bernal, F. J. Botana, J. J. Calvino, C. López, J. A. Pérez-Omil, J. M. Rodríguez-Izquierdo, High-resolution electron microscopy investigation of metal–support interactions in Rh/TiO₂. *J. Chem. Soc., Faraday Trans.* **92**, 2799–2809 (1996).
11. S. Zhang, P. N. Plessow, J. J. Willis, S. Dai, M. Xu, G. W. Graham, M. Cargnello, F. Abild-Pedersen, X. Pan, Dynamical Observation and Detailed Description of Catalysts under Strong Metal–Support Interaction. *Nano Lett.* **16**, 4528–4534 (2016).
12. J. Lee, S. P. Burt, C. A. Carrero, A. C. Alba-Rubio, I. Ro, B. J. O’Neill, H. J. Kim, D. H. K. Jackson, T. F. Kuech, I. Hermans, J. A. Dumesic, G. W. Huber, Stabilizing cobalt catalysts for aqueous-phase reactions by strong metal-support interaction. *J. Catal.* **330**, 19–27 (2015).
13. D. Liu, X. Y. Quek, W. N. E. Cheo, R. Lau, A. Borgna, Y. Yang, MCM-41 supported nickel-based bimetallic catalysts with superior stability during carbon dioxide reforming of methane: Effect of strong metal-support interaction. *J. Catal.* **266**, 380–390 (2009).
14. J. Li, Y. Lin, X. Pan, D. Miao, D. Ding, Y. Cui, J. Dong, X. Bao, Enhanced CO₂ Methanation Activity of Ni/Anatase Catalyst by Tuning Strong Metal–Support Interactions. *ACS Catal.* **9**, 6342–6348 (2019).
15. X. Liu, M.-H. Liu, Y.-C. Luo, C.-Y. Mou, S. D. Lin, H. Cheng, J.-M. Chen, J.-F. Lee, T.-S. Lin, Strong Metal–Support Interactions between Gold Nanoparticles and ZnO Nanorods in CO Oxidation. *J. Am. Chem. Soc.* **134**, 10251–10258 (2012).
16. T. Lunkenbein, J. Schumann, M. Behrens, R. Schlögl, M. G. Willinger, Formation of a ZnO Overlayer in Industrial Cu/ZnO/Al₂O₃ Catalysts Induced by Strong Metal-Support Interactions. *Angew. Chemie.* **127**, 4627–4631 (2015).
17. H. Tang, Y. Su, Y. Guo, L. Zhang, T. Li, K. Zang, F. Liu, L. Li, J. Luo, B. Qiao, J. Wang, Oxidative strong metal–support interactions (OMSI) of supported platinum-group metal

catalysts. *Chem. Sci.* **9**, 6679–6684 (2018).

18. S. Liu, W. Xu, Y. Niu, B. Zhang, L. Zheng, W. Liu, L. Li, J. Wang, Ultrastable Au nanoparticles on titania through an encapsulation strategy under oxidative atmosphere. *Nat. Commun.* **10**, 5790 (2019).

5 19. S. Liu, H. Qi, J. Zhou, W. Xu, Y. Niu, B. Zhang, Y. Zhao, W. Liu, Z. Ao, Z. Kuang, L. Li, M. Wang, J. Wang, Encapsulation of Platinum by Titania under an Oxidative Atmosphere: Contrary to Classical Strong Metal–Support Interactions. *ACS Catal.*, 6081–6090 (2021).

20. M. Tang, S. Li, S. Chen, Y. Ou, M. Hiroaki, W. Yuan, B. Zhu, H. Yang, Y. Gao, Z. Zhang, Y. Wang, Facet-Dependent Oxidative Strong Metal-Support Interactions of
10 Palladium–TiO₂ Determined by In Situ Transmission Electron Microscopy. *Angew. Chemie Int. Ed.* **60**, 22339–22344 (2021).

21. H. Tang, J. Wei, F. Liu, B. Qiao, X. Pan, L. Li, J. Liu, J. Wang, T. Zhang, Strong Metal–Support Interactions between Gold Nanoparticles and Nonoxides. *J. Am. Chem. Soc.* **138**, 56–59 (2016).

15 22. H. Tang, F. Liu, J. Wei, B. Qiao, K. Zhao, Y. Su, C. Jin, L. Li, J. J. Liu, J. Wang, T. Zhang, Ultrastable Hydroxyapatite/Titanium-Dioxide-Supported Gold Nanocatalyst with Strong Metal–Support Interaction for Carbon Monoxide Oxidation. *Angew. Chemie - Int. Ed.* **55**, 10606–10611 (2016).

23. A. K. Datye, M. Votsmeier, Opportunities and challenges in the development of advanced
20 materials for emission control catalysts. *Nat. Mater.* **20**, 1049–1059 (2021).

24. G. L. Haller, D. E. Resasco, in *Advances in Catalysis* (1989; <https://linkinghub.elsevier.com/retrieve/pii/S0360056408600188>), vol. 36, pp. 173–235.

25. A. Corma, P. Serna, P. Concepción, J. J. Calvino, Transforming Nonselective into Chemoselective Metal Catalysts for the Hydrogenation of Substituted Nitroaromatics. *J.*

Am. Chem. Soc. **130**, 8748–8753 (2008).

26. J. C. Matsubu, S. Zhang, L. DeRita, N. S. Marinkovic, J. G. Chen, G. W. Graham, X. Pan, P. Christopher, Adsorbate-mediated strong metal–support interactions in oxide-supported Rh catalysts. *Nat. Chem.* **9**, 120–127 (2017).

5 27. R. M. Kennedy, L. A. Crosby, K. Ding, C. P. Canlas, A. Gulec, L. D. Marks, J. W. Elam, C. L. Marshall, K. R. Poepelmeier, P. C. Stair, Replication of SMSI via ALD: TiO₂ Overcoats Increase Pt-Catalyzed Acrolein Hydrogenation Selectivity. *Catal. Letters.* **148**, 2223–2232 (2018).

10 28. M. Macino, A. J. Barnes, S. M. Althahban, R. Qu, E. K. Gibson, D. J. Morgan, S. J. Freakley, N. Dimitratos, C. J. Kiely, X. Gao, A. M. Beale, D. Bethell, Q. He, M. Sankar, G. J. Hutchings, Tuning of catalytic sites in Pt/TiO₂ catalysts for the chemoselective hydrogenation of 3-nitrostyrene. *Nat. Catal.* **2**, 873–881 (2019).

15 29. M. G. Willinger, W. Zhang, O. Bondarchuk, S. Shaikhutdinov, H.-J. Freund, R. Schlögl, A Case of Strong Metal-Support Interactions: Combining Advanced Microscopy and Model Systems to Elucidate the Atomic Structure of Interfaces. *Angew. Chemie Int. Ed.* **53**, 5998–6001 (2014).

30. S. Shaikhutdinov, Strong Metal–Support Interaction and Reactivity of Ultrathin Oxide Films. *Catal. Letters.* **148**, 2627–2635 (2018).

20 31. O. Dulub, W. Hebenstreit, U. Diebold, Imaging cluster surfaces with atomic resolution: The strong metal-support interaction state of pt supported on TiO₂(110). *Phys. Rev. Lett.* **84**, 3646–3649 (2000).

32. P. L. Hansen, J. B. Wagner, S. Helveg, J. R. Rostrup-Nielsen, B. S. Clausen, H. Topsøe, Atom-resolved imaging of dynamic shape changes in supported copper nanocrystals. *Science.* **295**, 2053–2055 (2002).

33. T. Altantzis, I. Lobato, A. De Backer, A. Béché, Y. Zhang, S. Basak, M. Porcu, Q. Xu, A. Sánchez-Iglesias, L. M. Liz-Marzán, G. Van Tendeloo, S. Van Aert, S. Bals, Three-Dimensional Quantification of the Facet Evolution of Pt Nanoparticles in a Variable Gaseous Environment. *Nano Lett.* **19**, 477–481 (2019).
- 5 34. H. Yoshida, K. Matsuura, Y. Kuwauchi, H. Kohno, S. Shimada, M. Haruta, S. Takeda, Temperature-dependent change in shape of platinum nanoparticles supported on CeO₂ during catalytic reactions. *Appl. Phys. Express.* **4**, 2–5 (2011).
35. Y. Kuwauchi, H. Yoshida, T. Akita, M. Haruta, S. Takeda, Intrinsic Catalytic Structure of Gold Nanoparticles Supported on TiO₂. *Angew. Chemie Int. Ed.* **51**, 7729–7733 (2012).
- 10 36. T. W. Hansen, Atomic-Resolution in Situ Transmission Electron Microscopy of a Promoter of a Heterogeneous Catalyst. *Science.* **294**, 1508–1510 (2001).
37. Y. Kuwauchi, S. Takeda, H. Yoshida, K. Sun, M. Haruta, H. Kohno, Stepwise Displacement of Catalytically Active Gold Nanoparticles on Cerium Oxide. *Nano Lett.* **13**, 3073–3077 (2013).
- 15 38. Y. Li, M. Kottwitz, J. L. Vincent, M. J. Enright, Z. Liu, L. Zhang, J. Huang, S. D. Senanayake, W. C. D. Yang, P. A. Crozier, R. G. Nuzzo, A. I. Frenkel, Dynamic structure of active sites in ceria-supported Pt catalysts for the water gas shift reaction. *Nat. Commun.* **12**, 1–9 (2021).
- 20 39. J. B. Wagner, F. Cavalca, C. D. Damsgaard, L. D. L. Duchstein, T. W. Hansen, Exploring the environmental transmission electron microscope. *Micron.* **43**, 1169–1175 (2012).
40. M. Plodinec, H. C. Nerl, R. Farra, M. G. Willinger, E. Stotz, R. Schlögl, T. Lunkenbein, Versatile Homebuilt Gas Feed and Analysis System for Operando TEM of Catalysts at Work. *Microsc. Microanal.*, 1–9 (2020).
41. M. Boniface, M. Plodinec, R. Schlögl, T. Lunkenbein, Quo Vadis Micro-Electro-

Mechanical Systems for the Study of Heterogeneous Catalysts Inside the Electron
Microscope? *Top. Catal.* **63**, 1623–1643 (2020).

42. A. Beck, M. Zabilskiy, M. A. Newton, O. Safonova, M. G. Willinger, J. A. Van
Bokhoven, Following the structure of copper-zinc-alumina across the pressure gap in
5 carbon dioxide hydrogenation. *Nat. Catal.* **4** (2021), doi:10.1038/s41929-021-00625-x.
43. W. Yuan, B. Zhu, K. Fang, X. Li, T. W. Hansen, Y. Ou, H. Yang, J. B. Wagner, Y. Gao,
Y. Wang, Z. Zhang, In situ manipulation of the active Au-TiO₂ interface with atomic
precision during CO oxidation. *Science*. **371**, 517–521 (2021).
44. J. Vincent, P. Crozier, Atomic-resolution Operando and Time-resolved In Situ TEM
10 Imaging of Oxygen Transfer Reactions Catalyzed by CeO₂-supported Pt Nanoparticles.
Microsc. Microanal. **26**, 1694–1695 (2020).
45. A. Akram, S. J. Freakley, C. Reece, M. Piccinini, G. Shaw, J. K. Edwards, F. Desmedt, P.
Miquel, E. Seuna, D. J. Willock, J. A. Moulijn, G. J. Hutchings, Gas phase stabiliser-free
production of hydrogen peroxide using supported gold-palladium catalysts. *Chem. Sci.* **7**,
15 5833–5837 (2016).
46. M. Chi, C. Wang, Y. Lei, G. Wang, D. Li, K. L. More, A. Lupini, L. F. Allard, N. M.
Markovic, V. R. Stamenkovic, Surface faceting and elemental diffusion behaviour at
atomic scale for alloy nanoparticles during in situ annealing. *Nat. Commun.* **6**, 8925
(2015).
- 20 47. J. Resasco, S. Dai, G. Graham, X. Pan, P. Christopher, Combining In-Situ Transmission
Electron Microscopy and Infrared Spectroscopy for Understanding Dynamic and Atomic-
Scale Features of Supported Metal Catalysts. *J. Phys. Chem. C.* **122**, 25143–25157 (2018).
48. X. Du, H. Tang, B. Qiao, Oxidative Strong Metal–Support Interactions. *Catalysts*. **11**, 896
(2021).

49. R. Vanselow, M. Mundschau, Diffusion and adsorption of titanium oxide on platinum as related to strong metal-support interactions. *J. Catal.* **103**, 426–435 (1987).
50. X. Xu, Q. Fu, L. Gan, J. Zhu, X. Bao, Interface-Confined FeOx Adlayers Induced by Metal Support Interaction in Pt/FeOx Catalysts. *J. Phys. Chem. B.* **122**, 984–990 (2018).
- 5 51. U. Diebold, The surface science of titanium dioxide. *Surf. Sci. Rep.* **48**, 53–229 (2003).
52. T. Kandemir, F. Girgsdies, T. C. Hansen, K.-D. Liss, I. Kasatkin, E. L. Kunkes, G. Wowsnick, N. Jacobsen, R. Schlögl, M. Behrens, In Situ Study of Catalytic Processes: Neutron Diffraction of a Methanol Synthesis Catalyst at Industrially Relevant Pressure. *Angew. Chemie Int. Ed.* **52**, 5166–5170 (2013).
- 10 53. A. Beck, H. Frey, M. Becker, L. Artiglia, M. G. Willinger, J. A. van Bokhoven, Influence of Hydrogen Pressure on the Structure of Platinum–Titania Catalysts. *J. Phys. Chem. C.* **125**, 22531–22538 (2021).
54. J. M. Hermann, M. Gravelle-Rumeau-Maillot, P. C. Gravelle, A microcalorimetric study of metal-support interaction in the Pt/TiO₂ system. *J. Catal.* **104**, 136–146 (1987).
- 15 55. G. B. Raupp, J. A. Dumesic, Adsorption of carbon monoxide, carbon dioxide, hydrogen, and water on titania surfaces with different oxidation states. *J. Phys. Chem.* **89**, 5240–5246 (1985).
56. C. Spreafico, W. Karim, Y. Ekinici, J. A. van Bokhoven, J. VandeVondele, Hydrogen Adsorption on Nanosized Platinum and Dynamics of Spillover onto Alumina and Titania. *J. Phys. Chem. C.* **121**, 17862–17872 (2017).
- 20 57. K. Zhang, L. Li, S. Shaikhutdinov, H.-J. J. Freund, Carbon Monoxide Oxidation on Metal-Supported Monolayer Oxide Films: Establishing Which Interface is Active. *Angew. Chemie - Int. Ed.* **57**, 1261–1265 (2018).
58. A. J. Fox, B. Drawl, G. R. Fox, B. J. Gibbons, S. Trolrier-McKinstry, Control of

crystallographic texture and surface morphology of Pt/TiO₂ templates for enhanced PZT thin film texture. *IEEE Trans. Ultrason. Ferroelectr. Freq. Control.* **62**, 56–61 (2015).

59. P. Müller, R. Kern, Equilibrium nano-shape changes induced by epitaxial stress (generalised Wulf–KaisheW theorem). *Surf. Sci.* **457**, 229–253 (2000).
- 5 60. C. Castellarin-Cudia, S. Surnev, G. Schneider, R. Podlucky, M. G. Ramsey, F. P. Netzer, Strain-induced formation of arrays of catalytically active sites at the metal–oxide interface. *Surf. Sci.* **554**, L120–L126 (2004).
61. A. Ruiz Puigdollers, P. Schlexer, S. Tosoni, G. Pacchioni, A. R. Puigdollers, P. Schlexer, S. Tosoni, G. Pacchioni, Increasing oxide reducibility: The role of metal/oxide interfaces
10 in the formation of oxygen vacancies. *ACS Catal.* **7**, 6493–6513 (2017).
62. J. L. Vincent, P. A. Crozier, Operando Insight into Oxygen Transfer at Pt/CeO₂ Interfaces during CO Oxidation. *Microsc. Microanal.* **25**, 1508–1509 (2019).
63. S. C. Ammal, A. Heyden, Modeling the noble metal/TiO₂ (110) interface with hybrid DFT functionals: A periodic electrostatic embedded cluster model study. *J. Chem. Phys.*
15 **133**, 164703 (2010).
64. C. Bäumer, R. Dittmann, in *Metal Oxide-Based Thin Film Structures* (Elsevier, 2018; <https://linkinghub.elsevier.com/retrieve/pii/B9780128111666000200>), pp. 489–522.
65. R. J. Kamaladasa, A. A. Sharma, Y.-T. T. Lai, W. Chen, P. A. Salvador, J. A. Bain, M. Skowronski, Y. N. Picard, In Situ TEM Imaging of Defect Dynamics under Electrical
20 Bias in Resistive Switching Rutile-TiO₂. *Microsc. Microanal.* **21**, 140–153 (2015).
66. D. S. Jeong, H. Schroeder, U. Breuer, R. Waser, Characteristic electroforming behavior in Pt/TiO₂/Pt resistive switching cells depending on atmosphere. *J. Appl. Phys.* **104**, 123716 (2008).
67. L. A. Bursill, B. G. Hyde, On the aggregation of wadsley defects in slightly reduced rutile.

Philos. Mag. **23**, 3–15 (1971).

68. L. A. Bursill, B. G. Hyde, D. K. Philp, New crystallographic shear families derived from the rutile structure, and the possibility of continuous ordered solid solution. *Philos. Mag. A J. Theor. Exp. Appl. Phys.* **23**, 1501–1513 (1971).

5 69. B. F. Donovan, D. M. Long, A. Moballeggh, N. Creange, E. C. Dickey, P. E. Hopkins, Impact of intrinsic point defect concentration on thermal transport in titanium dioxide. *Acta Mater.* **127**, 491–497 (2017).

70. M. D. Rasmussen, L. M. Molina, B. Hammer, Adsorption, diffusion, and dissociation of molecular oxygen at defected TiO₂(110): A density functional theory study. *J. Chem. Phys.* **120**, 988–997 (2004).

10 71. P. Liu, T. Wu, J. Madsen, J. Schiøtz, J. B. Wagner, T. W. Hansen, Transformations of supported gold nanoparticles observed by in situ electron microscopy. *Nanoscale.* **11**, 11885–11891 (2019).

72. W. Gao, Z. D. Hood, M. Chi, Interfaces in Heterogeneous Catalysts: Advancing
15 Mechanistic Understanding through Atomic-Scale Measurements. *Acc. Chem. Res.* **50**, 787–795 (2017).

73. P. Mars, D. W. van Krevelen, Oxidations carried out by means of vanadium oxide catalysts. *Chem. Eng. Sci.* **3**, 41–59 (1954).

74. R. Schaub, P. Thostrup, N. Lopez, E. Lægsgaard, I. Stensgaard, J. K. Nørskov, F.
20 Besenbacher, Oxygen Vacancies as Active Sites for Water Dissociation on Rutile TiO₂(110). *Phys. Rev. Lett.* **87**, 266104 (2001).

75. F. Pesty, H.-P. Steinrück, T. E. Madey, Thermal stability of Pt films on TiO₂(110): evidence for encapsulation. *Surf. Sci.* **339**, 83–95 (1995).

76. A. Wilson, A. Bailly, R. Bernard, Y. Borensztein, A. Coati, B. Croset, H. Cruguel, A.

Naitabdi, M. Silly, M.-C. Saint-Lager, A. Vlad, N. Witkowski, Y. Garreau, G. Prevot,
Gas-induced selective re-orientation of Au–Cu nanoparticles on TiO₂ (110). *Nanoscale*.
11, 752–761 (2019).

5

Acknowledgments:

Funding:

HF and MGW acknowledge the SNSF project 200021_181053, AB and JAvB acknowledge
the SNSF project 200021_178943.

10

Author contributions:

Conceptualization: MGW

Investigation: HF, AB, XH, MGW

Visualization: HF, MGW

15

Funding acquisition: MGW

Project administration: MGW, JAvB

Supervision: MGW, XH, JAvB,

Writing – original draft: HF, MGW

Writing – review & editing: MGW, HF, AB, XH, JAvB

20

Competing interests: Authors declare that they have no competing interests.

Data and materials availability: All data are available in the main text or the supplementary materials; addition details can be requested from the corresponding authors.

This is the accepted version of the following article: H. Frey, A. Beck, X. Huang, J. A. van Bokhoven, M. G. Willinger, Dynamic interplay between metal nanoparticles and oxide support under redox conditions. *Science*. **376**, 982–987 (2022), which has been published in final form at <https://www.science.org/doi/10.1126/science.abm3371>

Supplementary Materials: [science.org/doi/10.1126/science.abm3371](https://www.science.org/doi/10.1126/science.abm3371) Materials and Methods

10 **Supplementary Materials**

Materials and Methods

Supporting Figures 1 – 6

Supporting Movies 1 – 8

Reference (75, 76)

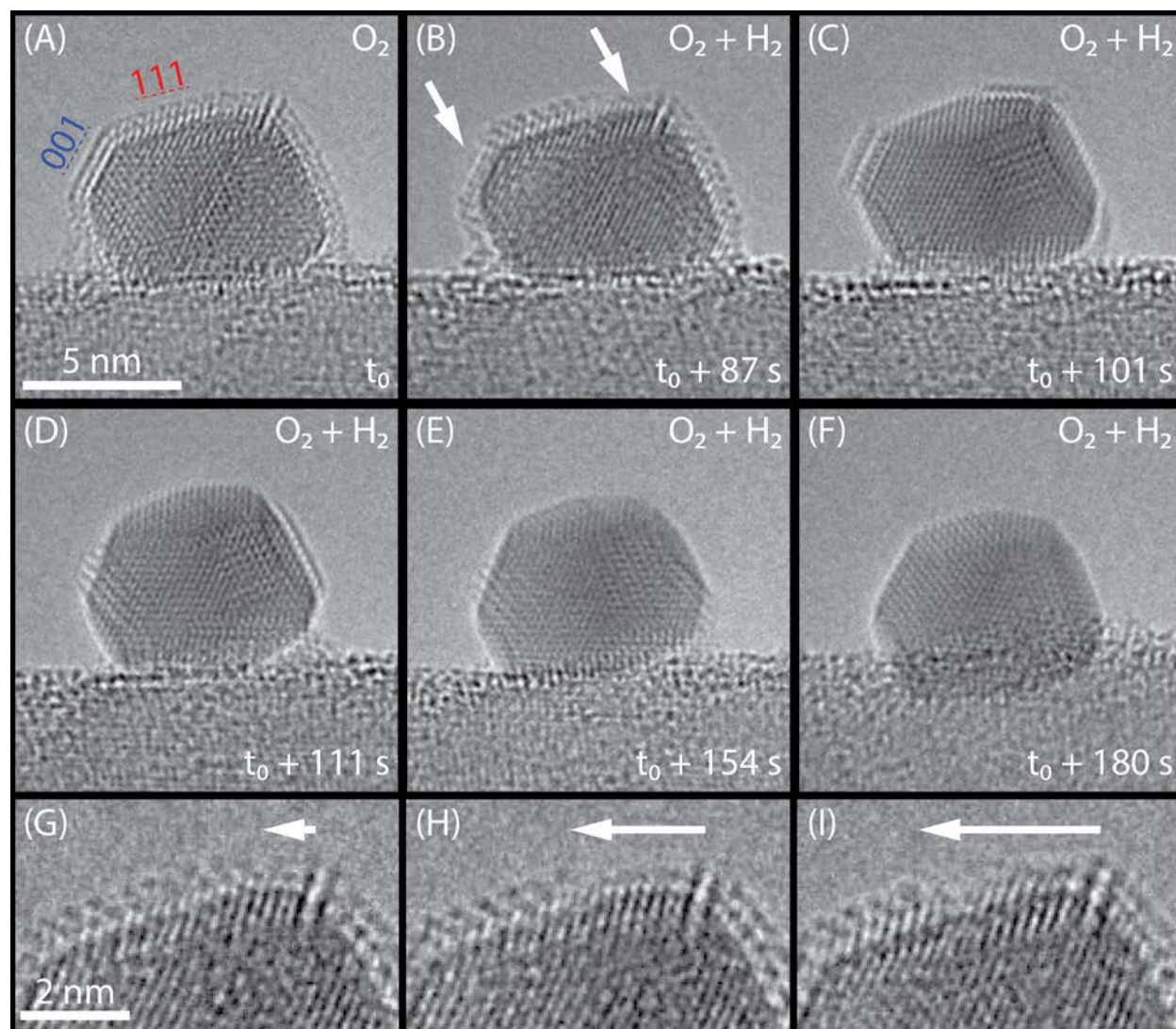


Fig. 1. Morphological change upon transition into redox active regime. (A to F) Images that were recorded while the composition of the gas-phase in the in situ gas-cell gradually changed from 700 mbar O₂ to a mixture of 60 mbar H₂ plus 700 mbar O₂. (G to I) Magnified images of the particle surface showing the gradual reduction of the overlayer between frames A and B. t₀ is the time at which the H₂ flow was turned on.

5

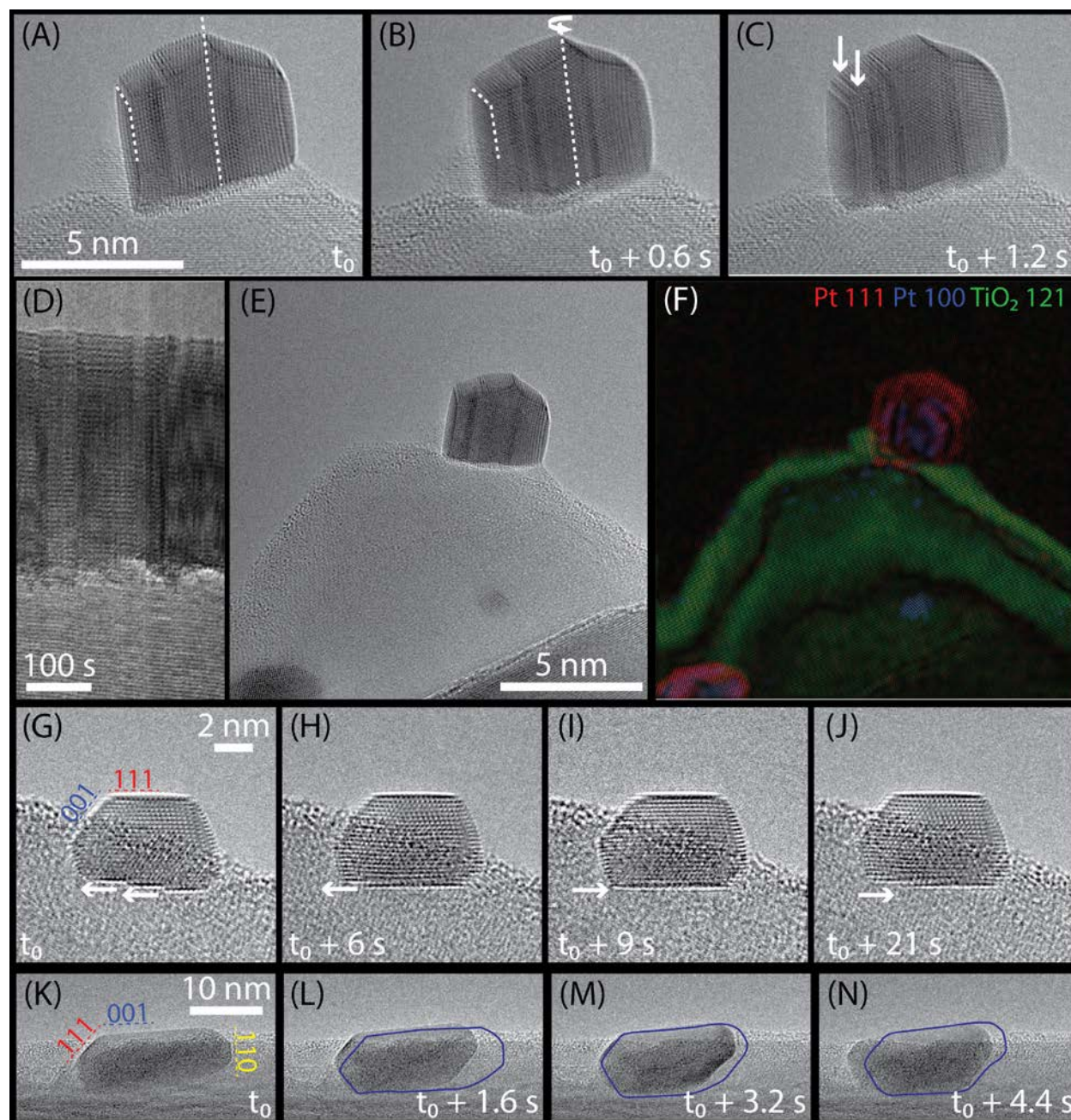


Fig. 2. Redox chemistry at the interface induces structural dynamics of Pt NPs and is the driving force for particle reconstruction and migration. (A to C) Individual frames of a movie recorded from a Pt NP that is oriented with {111} planes perpendicular to the interface. **(D)** View generated from the same movie by cutting a plane through the image stack along the time axis. It shows the up- and downward shifting of Pt{111} planes and associated collapse and reconstruction of the underlying TiO₂. **(E and F)** Image and its Fourier-filtered counterpart in which planes of

identical orientation appear in the same color: Green indicates (121) planes of TiO₂, red and blue to Pt(111) and Pt(100) planes, respectively. **(G to I)** Image sequence of a particle that is seemingly oriented with the Pt{111} planes parallel to the TiO₂ interface. **(K to N)** A NP that has its Pt{111} planes inclined toward the interface. The blue shape indicates the position of the Pt NP in the previous frame respectively.

5

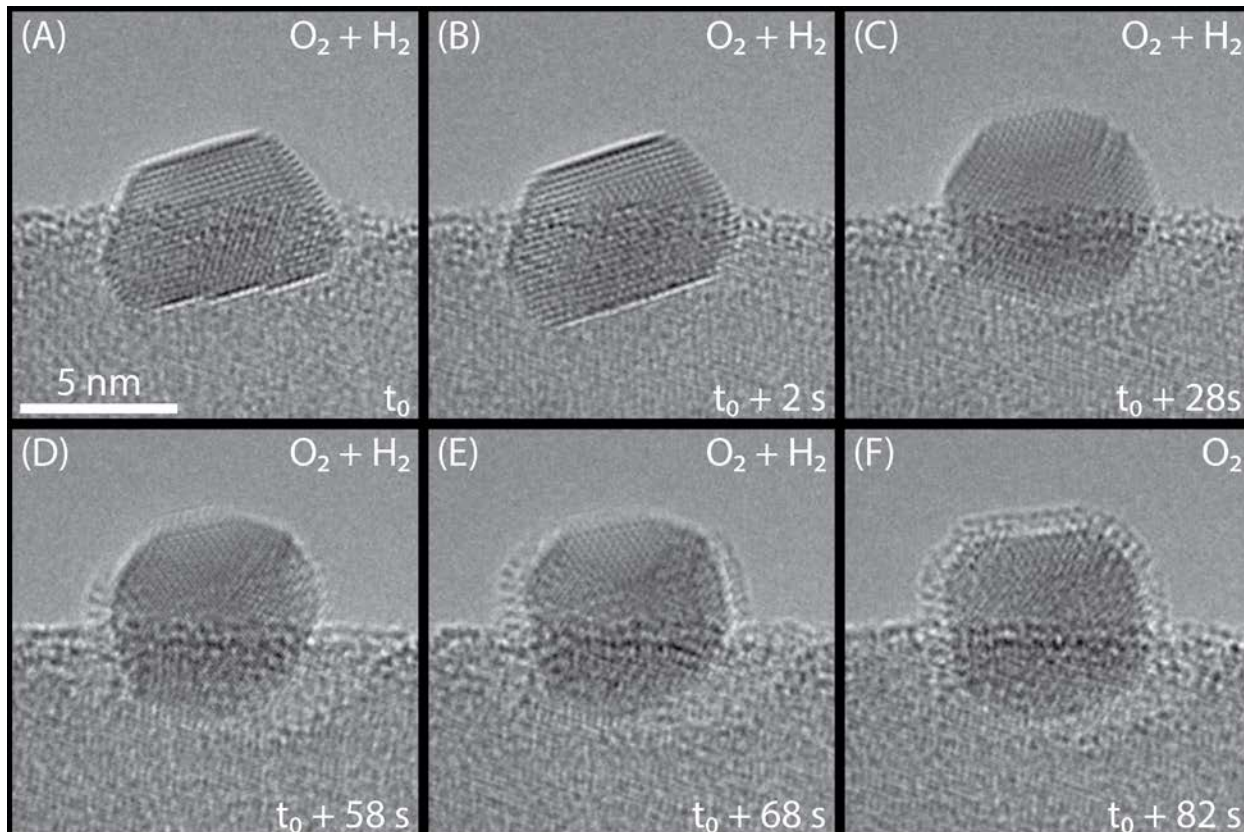


Fig. 3. Morphological change of a Pt NP upon leaving the redox active regime. Switching of the gas atmosphere from 60 mbar H₂ plus 700 mbar O₂ back to 700 mbar O₂ at 600 °C leads to reformation of a classical particle overgrowth. **(A to C)** The NP first adopted a spherical morphology. **(D to F)**. As soon as H₂ was fully removed from the reactor cell, the overlayer reformed from support material from the vicinity of the NP; t₀ is the time at which the H₂ flow was set to zero.

10

